Computational Mechanics (1992) 9, 233–247

Computational Mechanics

The 3D stress field of a fiber embedded into a matrix and subjected to an axial load

F. H. Zhong and **E. S. Folias**
Department of Mechanical Engineering, University of Utah, Salt Lake City, UT 84112, USA

Abstract. In this investigation, the 3D stress field of a single cylindrical fiber, which is embedded into a plate matrix, is examined. The composite body is subjected to an axial loading and both perfect imperfect bonding conditions at the interface are considered. The analysis, which is based on analytical considerations, reveals the load transfer characteristics from the fiber to the matrix and vice versa. Numerical results for the displacement and stress fields are given and shown to be sensitive to the diameter to thickness ratio, the respective material properties and the applied load ratio between the fiber and the matrix. Comparisons with available experimental data shows a very good agreement.

1 Introduction

It is well recognized that the mechanism of load transfer at the fiber/matrix interphase plays a major role in the mechanical and physical properties of composites. For this reason, a fundamental understanding and knowledge of the stress distribution induced by the applied load is essential, if one is to utilize these materials effectively. The subject has been investigated by a number of researchers and the results are reported in the literature. For example, two-dimensional solutions (plane stress and plane strain) for plates with perfectly bonded circular inclusions can be found in the papers of Sendeckyj (1970) and of Yu and Sendeckyj (1974). A general representation of the solution of an elastic curvilinear inclusion problem is presented by Sendeckyj. As an example, the authors consider an elliptical inclusion for discussion. The discussion is limited to the case of an infinite matrix. Later, the problem of an unbounded elastic matrix containing any number of elastic inclusions is solved by Yu et al. In both of these papers the use of a complex variable formulation is adopted. A more practical model for the mechanical behavior of unidirectional fiber-reinforced materials subjected to an axial loading is examined by Bloom (1967), where a hexagonal array of perfectly bonded filaments is assumed. Since these solutions are based on two-dimensional considerations, the effect of the thickness of the plate on the stress distributions could not be examined.

Three dimensional solutions to similar problems are not fully investigated due to the mathematical difficulties involved. Muki and Sternberg in 1970 investigated the diffusion of an axial load from a bar of arbitrary uniform cross-section that is immersed in, up to a finite depth, and bounded to a semi-infinite solid with distinct elastic properties. Their approximate method requires the radius of the rod to be small in comparison to its length. Luk and Keer in 1979 investigated a very similar problem. The rod bar at this time is assumed to be rigid. Many plots of the stresses based on numerical calculations are given. The authors have also examined what effect different parameters of the problem have on the stress field. It is important to note that all of the above works deal with one perfect isolated inclusion. On the other hand, in a fiber-reinforced composite thousands of fibers may be used to construct one layer of the laminate. Similar to the geometry of the problem examined by Bloom (1967), a three-dimensional solution is achieved by using the Boussinesq–Papkovitch potentials by Haener (1967). However, only few numerical results are presented in the paper. Perhaps the reason for this is the numerical complexity encountered as a result of the double summation. Folias in 1975 developed a method for constructing

solutions to some three-dimensional mixed boundary-value problems and applied it to the problem of a uniform extension of an infinite plate containing a through the thickness line crack. The general solution was, subsequently, used to investigate some related problems. In Penado and Folias (1989), the stress field around a cylindrical inclusion in a plate of arbitrary thickness is investigated, where a uniform tension is applied in the plane of the plate at points far remote from the inclusion. Since the thickness of the plate is no longer assumed to be infinite or semi-infinite, the results allow the examination of very thick and very thin plates and bridge the gap in between.

While all of the above discussions are restricted to the case where a perfect bonding condition prevails at the interface, there are few analytical models which deal with the imperfect bonding problem. The first model assumes that the inclusion and the plate are connected at the interface by an elastic spring. Tractions and displacements u and v are continuous across the interface, but the vertical displacement w may now be allowed to be discontinuous and the difference Δw is assumed to be proportional to the shear stress τ_{rz} at the interface. Papers by Lawrence (1972) and Banbaji (1988) approach the problem based on shear lag analysis and the results are, therefore, approximate. Most recent work done by Steif and Hoysan (1986) approaches the problem based on 2D considerations and the case in which the fiber and the matrix have identical elastic properties is solved. Numerical solutions for cases in which the fiber and the matrix have different elastic properties are obtained by a finite element method. The second model developed by Dollar and Steif (1988) assumes that the transfer of load at the interface is described by Coulomb friction. The mathematical models for stick, slip and separation conditions are given and the residual stress σ_{rr} is introduced into the discussion. Recently, Hutchinson and Jensen (1990) also considered models for possible debonding under the assumption of a (i) constant and (ii) Coulomb friction law. Their analysis is based on a cylinder model and approximate closed form solutions are presented. Haritos and Keer (1985) considered the problem of a finite, rigid insert partially embedded into and adhesively bonded to an elastic half space. The problem is then formulated in terms of a singular integral equation which is solved numerically. The fiber/matrix debonding problem with friction was also considered by Gao et al. (1988) based on an energy balance for fracture initiation. The interfacial friction is shown to have a significant effect on the debonded load. A similar work was also carried out later by Penn and Lee (1989). Shear lag models are used in both of these two papers in order to calculate the stress and the displacement fields. Finally, an interesting 2D model adopted by Achenbach and Zhu (1989) requires that the continuity of tractions and a linear relation between displacement differences be satisfied across the interphase and the conjugate tractions. Their analysis shows that a variation of the interphase parameters causes pronounced changes in the stress fields.

Some experimental work relating to the interface strength between a fiber and a matrix is presently available in the literature. For example, experiments carried out by Tyson and Davies (1965) on a two dimensional model of an aluminum alloy fiber into an Araldite resin provide photoelastic results for the interfacial shear stress. Also, pull-out experiments conducted by Chua and Piggott (1985) provided results for the interfacial yield strength and the interfacial work of fracture. Finally, some of the characteristics of load transfer and fracture in a single fiber/epoxy composite have been experimentally investigated by DiBenedetto et al. (1986). Their objective was to find a cumulative distribution of critical fiber lengths that may be used to calculate the interfacial shear strength.

The purpose of this investigation, is to examine the load transfer characteristics between a single fiber and a rectangular matrix based on 3D considerations. 3D elasticity will be used in order to capture any possible edge effects which may be present. At first, only the fiber will be allowed to carry an axial load. Subsequently, the matrix also will be allowed to carry a portion of the load. In both cases, perfect bonding will be assumed to prevail at the fiber/matrix interface. Finally, the interface will be assumed to be imperfectly bonded and will be allowed to slip. A fracture mechanics approach is beyond the scope of the present analysis. However, it is expected that the analysis will provide us with pertinent information relating to fracture. In order to simplify the mathematical complexities of our problem, the following assumptions will be made: (i). Both the plate and the inclusion are made of isotropic, homogeneous and linearly elastic materials, and (ii). Only one isolated inclusion is assumed to be embedded into the plate.

2 Formulation of the problems

2.1 Perfect bonding model 1

Consider a composite body consisting of a cylindrical fiber which is embedded into a matrix plate. The matrix plate occupies the space $|x| < \infty$, $|y| < \infty$, $|z| \leqq h$ and the fiber, or inclusion, has a radius $r = a$ and runs through the entire thickness of the plate matrix (see Fig. 1). For convenience, the region $r > a$ (plate) and the region $r < a$ (inclusion) are denoted by superscripts (1) and (2), respectively. As to loading, the fiber is assumed to carry a uniform tensile stress σ_0 along the direction of its axis. All other boundaries are assumed to be free of stress.

Perhaps it may be appropriate at this point to state the reasons for using a rectangular plate matrix. Such a geometry certainly represents a departure from the usual assumption of a cylinder or a shear lag model. Our main objective, however, it is to develop a method for constructing a 3D solution to a composite lamina in which a doubly periodic array of cylindrical fibers is embedded into. The present solution will then serve, in principle, as a Green's function for the more complex situation. From a mathematical point of view, the authors believe that it is extremely difficult to attack the latter problem directly. However, once the stress field due to one fiber has been recovered, it is "relatively" easy to extend the analysis to also include a periodic array of fibers. (It may be noted that the use of a cylinder model in this case satisfies the cell boundary conditions approximately.) Moreover, 3D theory of elasticity is used in order to recover any possible edge effects which may be present. Knowledge of such edge effects is essential in studying damage at straight edges, whole edges, fiber-bridging cracks, etc.

Returning next to the statement of the problem, in the absence of body forces, the coupled differential equations governing the displacements $u_k^{(i)}$ are:

$$\frac{m_i}{m_i - 2}\frac{\partial e^{(i)}}{\partial x_k} + \nabla^2 u_k^{(i)} = 0; \quad (k = 1, 2, 3; i = 1, 2), \tag{1}$$

where ∇^2 is the 3D Laplacian operator, $m_i = 1/\nu_i$, ν_i is Poisson's ratio and

$$e^{(i)} = \frac{\partial u_k^{(i)}}{\partial x_k}; \quad k = 1, 2, 3. \tag{2}$$

The stress-displacement relations are given by Hooke's law as:

$$\sigma_{kl}^{(i)} = 2\mu_i \left\{ \frac{1}{m_i - 2} e_{jj}^{(i)} \delta_{lk} + e_{lk}^{(i)} \right\}; \quad k, l = 1, 2, 3, \tag{3}$$

where μ_i are the respective shear moduli. As to the boundary conditions one must require that as $r \to \infty$;

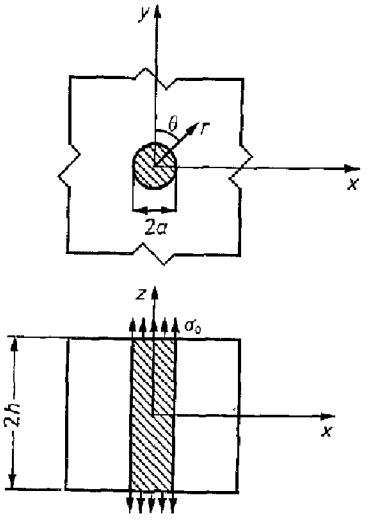

Fig. 1. Perfect bonding model 1: only fiber is subjected to an axial load

$$\sigma_{xx}^{(1)} = \sigma_{yy}^{(1)} = \sigma_{zz}^{(1)} = 0; \qquad \tau_{xy}^{(1)} = \tau_{yz}^{(1)} = \tau_{xz}^{(1)} = 0, \tag{4,5}$$

at $z = |h|$;

$$\tau_{xz}^{(1)} = \tau_{yz}^{(1)} = \sigma_{zz}^{(1)} = 0; \qquad \tau_{xz}^{(2)} = \tau_{yz}^{(2)} = 0; \qquad \sigma_{zz}^{(2)} = \sigma_0, \tag{6–8}$$

at $r = a$;

$$\sigma_{rr}^{(1)} - \sigma_{rr}^{(2)} = \tau_{r\theta}^{(1)} - \tau_{r\theta}^{(2)} = \tau_{rz}^{(1)} - \tau_{rz}^{(2)} = 0; \qquad u_{rr}^{(1)} - u_{rr}^{(2)} = u_{\theta\theta}^{(1)} - u_{\theta\theta}^{(2)} = u_{zz}^{(1)} - u_{zz}^{(2)} = 0. \tag{9,10}$$

In order to complete the formulation of the problem, one must also require that all stresses and displacements be finite at $r = 0$, i.e.

$$\lim_{r\to 0} \sigma_{lk}^{(i)} = \text{finite}, \quad \lim_{r\to 0} u_k^{(i)} = \text{finite}. \tag{11}$$

It is found convenient at this stage to seek the solution in the form:

$$u^{(i)} = u^{(p)(i)} + u^{(c)(i)}; \qquad v^{(i)} = v^{(p)(i)} + v^{(c)(i)}; \qquad w^{(i)} = w^{(p)(i)} + w^{(c)(i)}, \tag{12–14}$$

where the component with the superscript (p) represents the particular solution, and the component with the superscript (c) represents the complementary solution.

In general, the particular solution is relatively easy to obtain. It must satisfy the governing Eq. (1) as well as the boundary conditions far away from the inclusion. For the problem under consideration, the particular solution in cylindrical coordinates is:

(i) for the plate:

$$u_{rr}^{(p)(1)} = u_{\theta\theta}^{(p)(1)} = u_{zz}^{(p)(1)} = 0; \qquad \sigma_{rr}^{(p)(1)} = \sigma_{\theta\theta}^{(p)(1)} = \sigma_{zz}^{(p)(1)} = 0; \qquad \tau_{r\theta}^{(p)(1)} = \tau_{rz}^{(p)(1)} = \tau_{\theta z}^{(p)(1)} = 0, \tag{15–17}$$

(ii) for the inclusion:

$$u_{rr}^{(p)(2)} = C_1 r; \qquad u_{\theta\theta}^{(p)(2)} = 0; \qquad u_{zz}^{(p)(2)} = \left[\frac{\sigma_0}{2\mu_2}\frac{1-2\nu_2}{1-\nu_2} - \frac{2\nu_2}{1-\nu_2}C_1\right] z \tag{18–20}$$

$$\sigma_{rr}^{(p)(2)} = \sigma_{\theta\theta}^{(p)(1)} = \sigma_0 \frac{\nu_2}{1-\nu_2} + 2\mu_2 \frac{1+\nu_2}{1-\nu_2} C_1; \qquad \sigma_{zz}^{(p)(2)} = \sigma_0; \qquad \tau_{r\theta}^{(p)(2)} = \tau_{rz}^{(p)(2)} = \tau_{\theta z}^{(p)(2)} = 0, \tag{21–23}$$

where C_1 is a constant to be determined later from the boundary conditions of the complementary problem.

In view of the particular solution, one needs to find six complementary displacements $u^{(i)}$, $v^{(i)}$, $w^{(i)}$ $(i = 1, 2)$, such that they satisfy both the governing equations as well as the following boundary conditions:

at $|z| = h$;

$$\tau_{xz}^{(c)(i)} = \tau_{yz}^{(c)(i)} = \sigma_{zz}^{(c)(i)} = 0 \tag{24}$$

at $r = a$;

$$\sigma_{rr}^{(c)(1)} - \sigma_{rr}^{(c)(2)} = -\sigma_{rr}^{(p)(1)} + \sigma_{rr}^{(p)(2)}; \qquad \tau_{r\theta}^{(c)(1)} - \tau_{r\theta}^{(c)(2)} = -\tau_{r\theta}^{(p)(1)} + \tau_{r\theta}^{(p)(2)}, \tag{25,26}$$

$$\tau_{rz}^{(c)(1)} - \tau_{rz}^{(c)(2)} = \tau_{rz}^{(p)(1)} - \tau_{rz}^{(p)(2)}; \qquad u_{rr}^{(c)(1)} - u_{rr}^{(c)(2)} = -u_{rr}^{(p)(1)} + u_{rr}^{(p)(2)}, \tag{27,28}$$

$$u_{\theta\theta}^{(c)(1)} - u_{\theta\theta}^{(c)(2)} = -u_{\theta\theta}^{(p)(1)} + u_{\theta\theta}^{(p)(2)}; \qquad u_{zz}^{(c)(1)} - u_{zz}^{(c)(2)} = -u_{zz}^{(p)(1)} + u_{zz}^{(p)(2)}. \tag{29,30}$$

While it is well recognized that some academic liberty was taken in assuming that a uniform stress loading condition exists on the fiber surface, nevertheless the results are still expected to be valid outside the region of one fiber diameter away from the fiber edge (Folias 1991). The approximation, however, reduces the mathematical complexities of the problem considerably. Once the present solution has been obtained, it is then relatively easy to extend the analysis to also include other, physically, more realistic stress loading profiles of the type shown in Fig. 2. (At such edges, it has been shown that a weak stress singularity is present (see Folias (1991) for a glass fiber, Li and Folias, 1991 for a carbon fiber).) This matter is presently under investigation and the results will be reported in a follow-up short note.

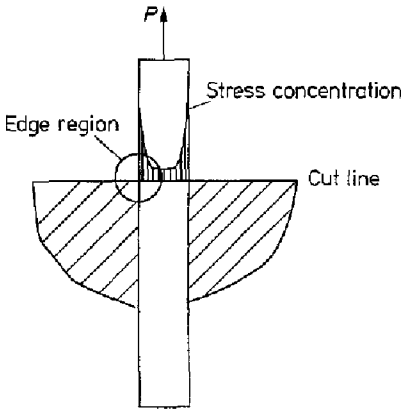

Fig. 2. Perfect bonding model 1 with a stress riser effect ad edge region

2.2 *Perfect bonding model 2*

In the previous section we discussed the case where only the fiber carries the load and where the surfaces of the matrix plate are free of stress. Such model, is most often used to illustrate the mechanics of load transfer from a fiber to a matrix. In other applications, however, both fiber and matrix may carry portions of the external load (e.g., a unidirectional composite plate). For this reason, we consider in Fig. 3 a modified model which allows the matrix plate to carry also an axial load σ_i. From a practical point of view, the magnitude of σ_i will be less than σ_0.

Thus, most of the formulas developed for perfect bonding model 1 are still valid with the exception of the following modifications to Eqs. (15–17).

$$u_{rr}^{(p)(1)} = -\frac{\sigma_i}{2\mu_1(m_1+1)}r; \qquad u_{\theta\theta}^{(p)(1)} = 0, \tag{31,32}$$

$$u_{zz}^{(p)(1)} = \frac{m_1\sigma_i}{2\mu_1(m_1+1)}z; \qquad \sigma_{rr}^{(p)(1)} = \sigma_{\theta\theta}^{(p)(1)} = 0, \tag{33,34}$$

$$\sigma_{zz}^{(p)(1)} = \sigma_i; \qquad \tau_{r\theta}^{(p)(1)} = \tau_{rz}^{(p)(1)} = \tau_{\theta z}^{(p)(1)} = 0. \tag{35,36}$$

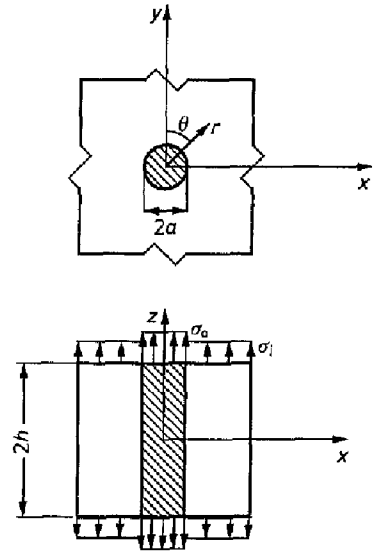

3

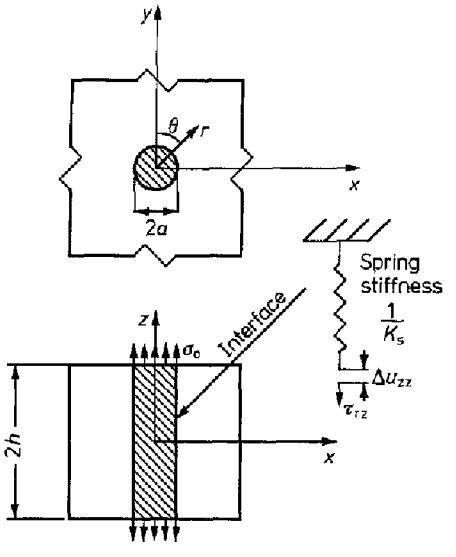

4

Figs. 3 and 4. 3 Perfect bonding model 2: both fiber and matrix are subjected to axial loads. 4 Imperfect bonding model: elastic spring present at the interface

2.3 *Imperfect bonding model*

Conditions of perfect bonding require that both displacements and stresses be continuous across the interface and throughout the thickness. Since both of the above models satisfy Eqs. (9) and (10), we define them as perfect bonding cases. As it was previously noted, imperfect bonding models which have been examined based on 2D considerations are basically of two types: in the first type the transfer of load across the interface is described by Coulomb friction, while in the second type, the transfer of load across the interface is described by a continuous elastic spring which connects the fiber and the matrix. In this analysis, we choose the latter for it is more suitable with the structure of our complementary solution.

This particular model is shown schematically in Fig. 4. Crucial to the problem of interest is the bonding between the fiber and the matrix at $r = a$ where the relevant stresses, as well as the displacements u and v, must be continuous. The vertical displacement w, however, is allowed to have a jump which is proportional to the shear stress i.e., at $r = a$:

$$u_{zz}^{(1)} - u_{zz}^{(2)} = K_s \tau_{rz}^{(i)}; \quad (i = 1 \text{ or } 2) \tag{37}$$

where $1/K_s$ denotes the shear stiffness at the interface. Mathematically, however, such a boundary condition is somewhat peculiar, at least in the neighborhood of $z = h$, where the displacement is non-singular while the shear stress is singular (Here it is assumed that insufficient slippage has taken place and that although the singularity strength has decreased, it has not totally been eliminated) see Folias 1989, 1991). Be that as it may, outside the boundary layer region (i.e., one fiber diameter away from the surface), the results are expected to be mathematically valid and it is hoped that they will provide us with some further insight on the question of friction. This matter will be discussed further in a later section. Finally, in terms of the complementary and particular solutions, the boundary condition (37) becomes

$$u_{zz}^{(c)(1)} - u_{zz}^{(c)(2)} = -u_{zz}^{(p)(1)} + u_{zz}^{(p)(2)} + K_s \tau_{rz}^{(i)}, \tag{38}$$

while all other boundary conditions remain the same. It remains, therefore, for us to find a complementary solution such that it satisfies Navier's equations and the appropriate boundary conditions.

3 Method of solution

A general method for constructing solutions to some 3D mixed boundary-value problems has been developed by Folias (1975), and a general solution has been constructed and subsequently put in a more convenient form for use in practical applications (Folias and Reuter 1990). The latter reference also addresses the question of the completeness of the eigenfunctions. Thus, without going into the mathematical details, one may now write the complementary solution in the form:

$$u^{(c)(i)} = \frac{1}{m_i - 2} \sum_{\nu=1}^{\infty} \frac{\partial^2 H_\nu^{(i)}}{\partial x^2} \{2(m_i - 1) f_1(\beta_\nu z) + m_i f_2(\beta_\nu z)\} + \lambda_1^{(i)} - y \frac{\partial \lambda_3^{(i)}}{\partial x} + \frac{1}{m_i + 1} z^2 \frac{\partial^2 \lambda_3^{(i)}}{\partial x \partial y}, \tag{39}$$

$$v^{(c)(i)} = \frac{1}{m_i - 2} \sum_{\nu=1}^{\infty} \frac{\partial^2 H_\nu^{(i)}}{\partial x \partial y} \{2(m_i - 1) f_1(\beta_\nu z) + m_i f_2(\beta_\nu z)\} + \frac{3m_i - 1}{m_i + 1} \lambda_3^{(i)} + \lambda_2^{(i)} - y \frac{\partial \lambda_3^{(i)}}{\partial y} - \frac{1}{m_i + 1} z^2 \frac{\partial^2 \lambda_3^{(i)}}{\partial x^2}, \tag{40}$$

$$w^{(c)(i)} = \frac{1}{m_i - 2} \sum_{\nu=1}^{\infty} \frac{\partial H_\nu^{(i)}}{\partial x} \{(m_i - 2) f_3(\beta_\nu z) - m_i f_4(\beta_\nu z)\} - \frac{2}{m_i + 1} z \frac{\partial \lambda_3^{(i)}}{\partial x}. \tag{41}$$

Furthermore the stresses are given by Hooke's law as:

$$\frac{1}{2\mu_i} \sigma_{xx}^{(c)(i)} = \frac{1}{m_i - 2} \sum_{\nu=1}^{\infty} \left\{ 2\beta_\nu^2 \frac{\partial H_\nu^{(i)}}{\partial x} f_1(\beta_\nu z) + \frac{\partial^3 H_\nu^{(i)}}{\partial x^3} [2(m_i - 1) f_1(\beta_\nu z) + m_i f_2(\beta_\nu z)] \right\}$$
$$+ \frac{\partial \lambda_1^{(i)}}{\partial x} - y \frac{\partial^2 \lambda_3^{(i)}}{\partial x^2} + \frac{2}{m_i + 1} \frac{\partial \lambda_3^{(i)}}{\partial y} + \frac{1}{m_i + 1} z^2 \frac{\partial^3 \lambda_3^{(i)}}{\partial x^2 \partial y}, \tag{42}$$

$$\frac{1}{2\mu_i}\sigma_{yy}^{(c)(i)} = \frac{1}{m_i-2}\sum_{\nu=1}^{\infty}\left\{2\beta_\nu^2\frac{\partial H_n^{(i)}}{\partial x}f_1(\beta_\nu z) - \left(\frac{\partial^3 H_\nu^{(i)}}{\partial x^3} - \beta_\nu^2\frac{\partial H_\nu^{(i)}}{\partial x}\right)[2(m_i-1)f_1(\beta_\nu z) + m_i f_2(\beta_\nu z)]\right\}$$
$$-\frac{\partial\lambda_1^{(i)}}{\partial x} + y\frac{\partial^2\lambda_3^{(i)}}{\partial x^2} + \frac{2m_i}{m_i+1}\frac{\partial\lambda_3^{(i)}}{\partial x} - \frac{1}{m_i+1}z^2\frac{\partial^3\lambda_3^{(i)}}{\partial x^2\partial y}, \tag{43}$$

$$\frac{1}{2\mu_i}\sigma_{zz}^{(c)(i)} = -\frac{m_i}{m_i-2}\sum_{\nu=1}^{\infty}\frac{\partial H_\nu^{(i)}}{\partial x}\beta_\nu^2 f_2(\beta_\nu z), \tag{44}$$

$$\frac{1}{2\mu_i}\tau_{xy}^{(c)(i)} = \frac{1}{m_i-2}\sum_{\nu=1}^{\infty}\frac{\partial^3 H_\nu^{(i)}}{\partial x^2\partial y}\{2(m_i-1)f_1(\beta_\nu z) + m_i f_2(\beta_\nu z)\}$$
$$+\frac{\partial\lambda_2^{(i)}}{\partial x} + y\frac{\partial^2\lambda_3^{(i)}}{\partial x\partial y} + \frac{m_i-1}{m_i+1}\frac{\partial\lambda_3^{(i)}}{\partial x} - \frac{1}{m_i+1}z^2\frac{\partial^3\lambda_3^{(i)}}{\partial x^3}, \tag{45}$$

$$\frac{1}{2\mu_i}\tau_{yz}^{(c)(i)} = -\frac{m_i}{m_i-2}\sum_{\nu=1}^{\infty}\frac{\partial^2 H_\nu^{(i)}}{\partial x\partial y}\beta_\nu\{f_3(\beta_\nu z) + f_4(\beta_\nu z)\}, \tag{46}$$

$$\frac{1}{2\mu_i}\tau_{xz}^{(c)(i)} = -\frac{m_i}{m_i-2}\sum_{\nu=1}^{\infty}\frac{\partial^2 H_\nu^{(i)}}{\partial x^2}\beta_\nu\{f_3(\beta_\nu z) + f_4(\beta_\nu z)\}, \tag{47}$$

where

$$\alpha_n = \frac{n\pi}{h}, \quad n = 1, 2, 3, \ldots, \tag{48}$$

β_ν are the roots of the equation

$$\sin(2\beta_\nu h) = -2\beta_\nu h, \tag{49}$$

$H_\nu^{(i)}$ $(i = 1, 2)$ are functions of x and y which satisfy the reduced wave equation:

$$\left(\frac{\partial^2}{\partial x^2} + \frac{\partial^2}{\partial y^2} - \beta_\nu^2\right)H_\nu^{(i)} = 0, \tag{50}$$

$\lambda_1^{(i)}$, $\lambda_2^{(i)}$ and $\lambda_3^{(i)}$ are two dimensional harmonic functions, and

$$f_1(\beta_\nu z) = \cos(\beta_\nu h)\cos(\beta_\nu z); \qquad f_2(\beta_\nu z) = \beta_\nu h\sin(\beta_\nu h)\cos(\beta_\nu z) - \beta_\nu z\cos(\beta_\nu h)\sin(\beta_\nu z), \tag{51, 52}$$

$$f_3(\beta_\nu z) = \cos(\beta_\nu h)\sin(\beta_\nu z); \qquad f_4(\beta_\nu z) = \beta_\nu h\sin(\beta_\nu h)\sin(\beta_\nu z) + \beta_\nu z\cos(\beta_\nu h)\cos(\beta_\nu z). \tag{53, 54}$$

The reader may notice that the above complementary solution automatically satisfies the boundary conditions at $|z| = h$ and that only the boundary conditions at the interface $r = a$ remain to be satisfied.

Taking advantage of the symmetry which the problem possesses, we write the extended boundary conditions in terms of the cylindrical coordinates r, θ and z. Thus, Eqs. (25–30) may be written in the following form:

$$\sin^2\theta(\sigma_{xx}^{(c)(1)} - \sigma_{xx}^{(c)(2)}) + \cos^2\theta(\sigma_{yy}^{(c)(1)} - \sigma_{yy}^{(c)(2)}) + \sin(2\theta)(\tau_{xy}^{(c)(1)} - \tau_{xy}^{(c)(2)}) = \sigma_0\frac{\nu_2}{1-\nu_2} + 2\mu_2\frac{1+\nu_2}{1-\nu_2}C_1 \tag{55}$$

$$\tfrac{1}{2}\sin 2\theta(\sigma_{xx}^{(c)(1)} - \sigma_{xx}^{(c)(2)}) - \tfrac{1}{2}\sin 2\theta(\sigma_{yy}^{(c)(1)} - \sigma_{yy}^{(c)(2)}) + \cos(2\theta)(\tau_{xy}^{(c)(1)} - \tau_{xy}^{(c)(2)}) = 0 \tag{56}$$

$$\sin\theta(\tau_{xz}^{(c)(1)} - \tau_{xz}^{(c)(2)}) + \cos\theta(\tau_{yz}^{(c)(1)} - \tau_{yz}^{(c)(2)}) = 0 \tag{57}$$

$$\sin\theta(u^{(c)(1)} - u^{(c)(2)}) + \cos\theta(v^{(c)(1)} - v^{(c)(2)}) = C_1 a + \frac{\sigma_i}{2\mu_1(m_1+1)}a \tag{58}$$

$$\cos\theta(u^{(c)(1)} - u^{(c)(2)}) - \sin\theta(v^{(c)(1)} - v^{(c)(2)}) = 0 \tag{59}$$

$$w^{(c)(1)} - w^{(c)(2)} = \left[\frac{\sigma_0}{2\mu_2}\frac{1-2\nu_2}{1-\nu_2} - \frac{2\nu_2}{1-\nu_2}C_1\right]z - \frac{m_1\sigma_i}{2\mu_1(m_1+1)}z. \tag{60}$$

Inasmuch as model 1 is a special case of model 2 where $\sigma_i = 0$, from here on one only needs to concentrate on the construction of the solution to model 2.

Taking into account the symmetry of the problem (θ independence), we let

$$\frac{\partial H_\nu^{(1)}}{\partial x} = C_{1\nu} K_0(\beta_\nu r); \qquad \frac{\partial H_\nu^{(2)}}{\partial x} = C_{2\nu} I_0(\beta_\nu r) \tag{61,62}$$

and all $\lambda = 0$ except

$$\lambda_1^{(1)} = \frac{A}{r}\sin\theta; \qquad \lambda_2^{(1)} = \frac{A}{r}\cos\theta, \tag{63,64}$$

where I_0 and K_0 are, respectively, the modified Bessel functions of the first and second kind of order zero; $C_{1\nu}$ and $C_{2\nu}$ are complex constants. The constants A and C_1 are to be determined in such a way that all remaining boundary conditions are satisfied.

4 Numerical results

Omitting the long and tedious numerical details, the problem is reduced to a system of six equations involving series in z, which are then solved numerically for the unknown coefficients. Perhaps it is noteworthy to note that the system is sensitive to small changes and for this reason double precision is used throughout the numerical analysis.

Once the coefficients have been determined, the displacement and stresses may then be calculated at any point of the composite body.

4.1 Perfect bonding model 1

Inasmuch as the interface is of greatest practical interest, plots at $r = a$ are given for the displacements and stresses as functions of z. The case of perfect bonding (model 1) will be taken as the basis of our first discussion. Two different shear moduli ratios are chosen: these are $\mu_2/\mu_1 = 2$ and $\mu_2/\mu_1 = 17$ corresponding to (a) and (b) respectively in each figure. The purpose of these plots is to examine how the shear moduli ratio affects the displacement and stress fields. Each plot consists of several curves which correspond to different a/h ratios. Superscripts are used to distinguish whether the stress or displacement is in the fiber or in the matrix as they have been defined early in the Fig. 1. However the superscripts are omitted if the stress or displacement is the same for both fiber and matrix at the interface.

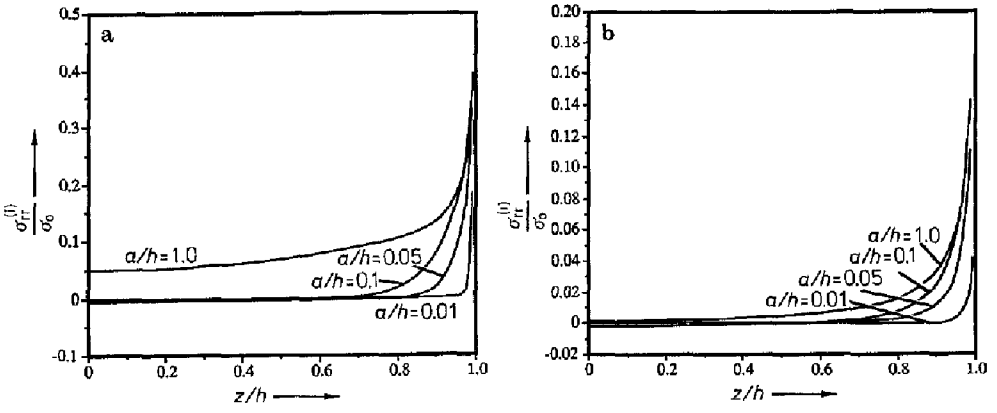

Fig. 5 a and b. Stress σ_{rr} vs z/h for perfect bonding model 1 where **a** corresponds to $\mu_2/\mu_1 = 2$ and $\nu_1 = \nu_2 = 0.33$ **b** corresponds to $\mu_2/\mu_1 = 17$ and $\nu_1 = \nu_2 = 0.33$

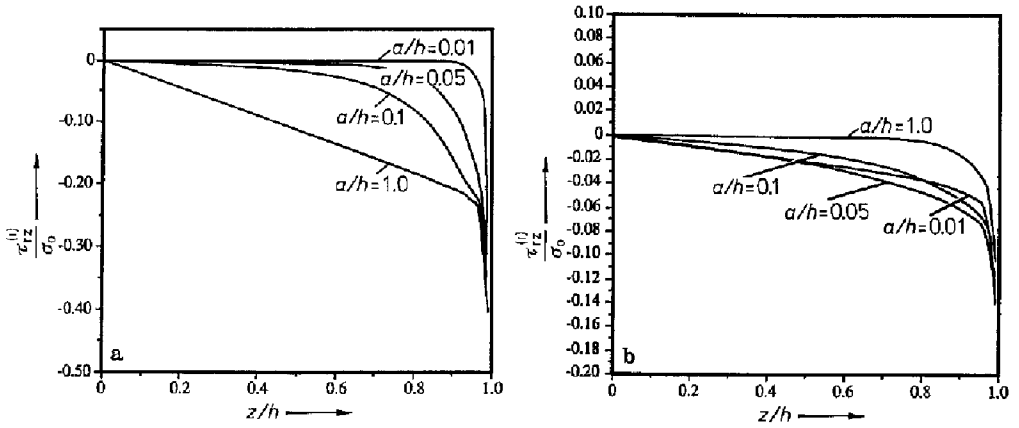

Fig. 6 a and b. Stress τ_{rz} vs z/h for perfect bonding model 1 where **a** corresponds to $\mu_2/\mu_1 = 2$ and $\nu_2 = 0.33$ **b** corresponds to $\mu_2/\mu_1 = 17$ and $\nu_1 = \nu_2 = 0.33$

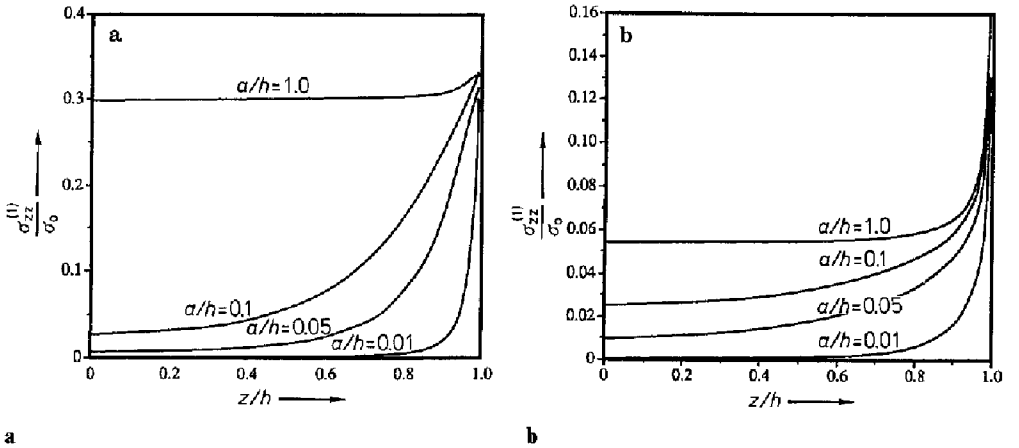

Fig. 7 a and b. Stress $\rho_{zz}^{(1)}$ vs z/h for perfect bonding model 1 where **a** corresponds to $\mu_2/\mu_1 = 2$ and $\nu_1 = \nu_2 = 0.33$ **b** corresponds to $\mu_2/\mu_1 = 17$ and $\nu_1 = \nu_2 = 0.33$

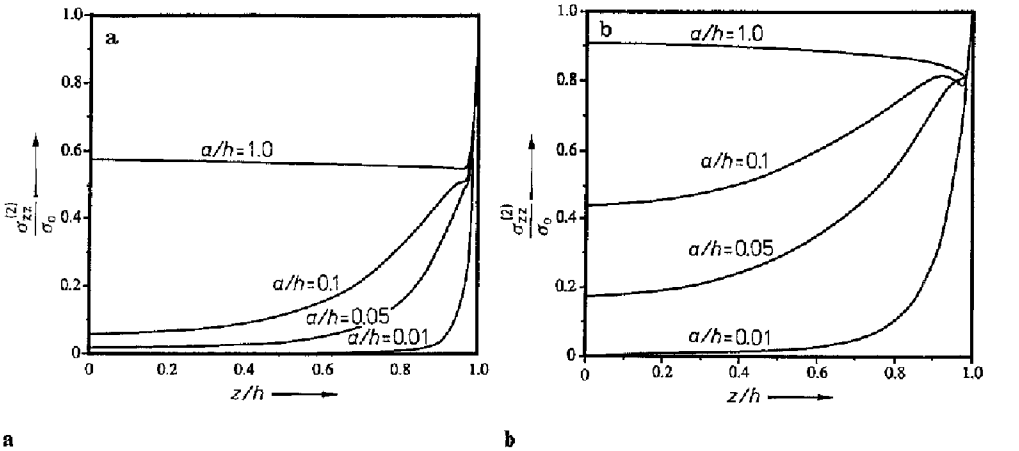

Fig. 8 a and b. Stress $\sigma_{zz}^{(2)}$ vs z/h for perfect bonding model 1 where **a** corresponds to $\mu_2/\mu_1 = 2$ and $\nu_1 = \nu_2 = 0.33$ **b** corresponds to $\mu_2/\mu_1 = 17$ and $\nu_1 = \nu_2 = 0.33$

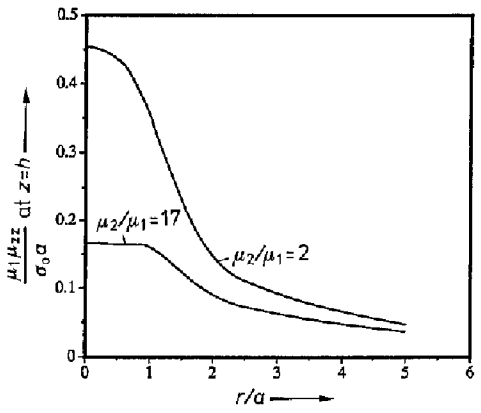

Fig. 9. Displacement u_{zz} at $z = h$ vs r/a for perfect bonding model 1 where $\nu_1 = \nu_2 = 0.33$ and $a/h = 0.05$

The radial stress profile is shown in Figs. 5a and b as a function of z/h. It is noted that, along the central region, the radial stress is almost constant and that it increases rather rapidly as one approaches the fiber edge. The results suggest, therefore, the presence of a boundary layer in which the stresses posses a weak singularity (Folias, 1989). The thickness of this boundary layer is approximately five fiber diameter away from the edge. It is interesting to note that for small a/h ratios, the radial stress is slightly negative over a wide span across the central region. This suggests, therefore, that in this region a small state of compression exists at the interface between the fiber and the matrix. Alternatively, for large a/h ratios, the radial stress is slightly positive and the interface is in a state of tension.

The interface shear stress exhibits a similar stress profile and is given in Figs. 6a and b. The sign for the shear stress is negative because the shear stress will always be opposing the direction of the external stress σ_0 applied at the edge of the fiber. The variation of the magnitude of the shear stress τ_{rz} seems more complicated in the case where $\mu_2/\mu_1 = 17$, than in the case where $\mu_2/\mu_1 = 2$. The former (Fig. 6b) shows the shear stress to reverse as a/h increases beyond a certain value. It appears that both "very thick" and "very thin" matrix plates will induce a very small shear stress along the center region. The matrix stress $\sigma_{zz}^{(1)}$ at the interface is plotted in Figs. 7a and b. Note that the stress increases as the ratio of a/h increases and that a large load may cause the fiber/matrix interface to debond at the fiber end. For most cases, the stress $\sigma_{zz}^{(2)}$ shown in Figs. 8a and b decays as one moves from the fiber end ($z = h$) to the fiber center ($z = 0$). However for all cases where $a/h = 1.0$, the analysis shows that the stress increases as one reaches the fiber center. It is also noted that the tensile stress at the matrix will decrease as μ_2/μ_1 increases by comparing Fig. 7b with Fig. 7a while the tensile stress at the fiber will increase by comparing Fig. 8b with Fig. 8a. This suggests that the load diffusion from the fiber to the matrix will decrease as the fiber becomes stiffer. Finally, the displacement u_{zz} at $z = h$ vs the radial distance is given in Fig. 9 where it is seen that a softer fiber ($\mu_2/\mu_1 = 2$) gives a smoother connection of the displacement at $r = a$, while a stiffer fiber ($\mu_2/\mu_1 = 17$) gives a sharper connection of the displacement at the interface.

4.2 Perfect bonding model 2

Inasmuch as, in practice, the matrix also carries a small portion of the applied load, it is desirable now to extend our model to the case where the matrix may also carry part of the load in the direction of the fiber length. Thus, perfect bonding model 2 allows us to examine how the load is being transferred from the fiber to the matrix and vice versa. In order to examine the effect of the matrix load σ_i on the stress field (see Fig. 3), the shear moduli ratio is chosen as $\mu_2/\mu_1 = 17$ and the geometric parameter a/h is fixed at $a/h = 0.05$. Three curves are plotted in each figure, which correspond to $\sigma_i/\sigma_0 = 0.0$, 0.05 and 0.1, respectively. It should be emphasized that the ratio σ_i/σ_0 is not an independent parameter. Actually this ratio will depend on the shear moduli ratio μ_2/μ_1, if a uniform

strain is assumed at the surface of the fiber and of the matrix. Thus, for the parameters chosen, a more realistic ratio of σ_i/σ_0 should be around 1/17.

In Figs. 10 and 11 we plot the radial and shear stresses as a function of z/h. Notice the reversal of the sign, as the ratio of σ_i/σ_0 increases from 0 to 0.1. Such sign reversal will most likely have implications to the process of debonding at the fiber/matrix interface. Finally, Fig. 12 shows the stress profile $\sigma_{zz}^{(2)}$ at the interface to dramatically increase as the ratio of σ_i/σ_0 increases.

4.3 Imperfect bonding case

Once the interface has been allowed to slip, the magnitude of the stresses in the matrix will be expected to decrease while the stresses in the fiber will be expected to increase slightly. In order to show the effect of stiffness of the interface, two parameters are fixed: they are $a/h = 0.05$ and $\mu_2/\mu_1 = 17$. Three curves, which correspond to the reciprocal of the spring constants $K_e = 0.0$, 0.1 and 1.0, are plotted (The reader may note that $\sigma_i = 0$ for this case).

The radial stress σ_{rr} shown in Fig. 13 increases slightly as the interface becomes softer (note $K_e = 0$ corresponds to perfect bonding case, or, the rigid interface). This indicates that a softer interface will increase the chance of interfacial debonding. On the other hand, the shear stress τ_{rz} shown in Fig. 14 exhibits a dramatic decrease of the magnitude of the stress along the interface. Similarly, the fiber tensile stress $\sigma_{zz}^{(2)}$ (Fig. 15) increases as slippage is allowed to increase. This suggests, therefore, that a lesser load will be transferred from the fiber to the matrix when the interface is softer, a result which is compatible with our expectation. As a practical matter, the spring constant may now be calculated by the equations given by Stief and Hoysan (1986), where a coated fiber model and a interfacial crack model are considered. Moreover, they point out that

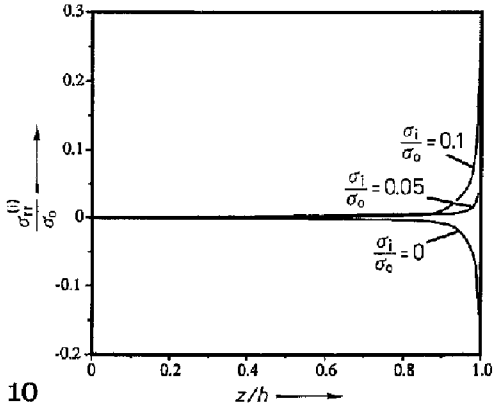

10

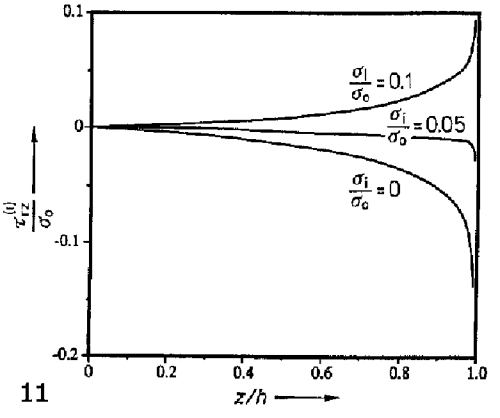

11

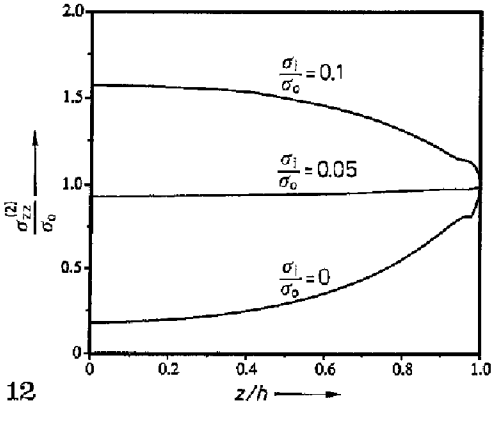

12

Figs. 10–12. 10 Stress σ_{rr} vs z/h, **11** stress τ_{rz} vs z/h, **12** stress $\sigma_{zz}^{(2)}$ vs z/h, all for perfect bonding model 2 where $\nu_1 = \nu_2 = 0.33$, $\mu_2/\mu_1 = 17$ and $a/h = 0.05$

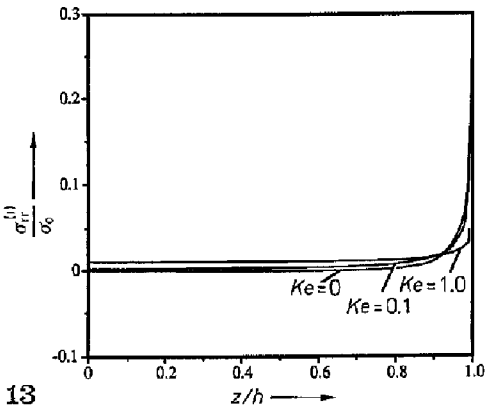

13

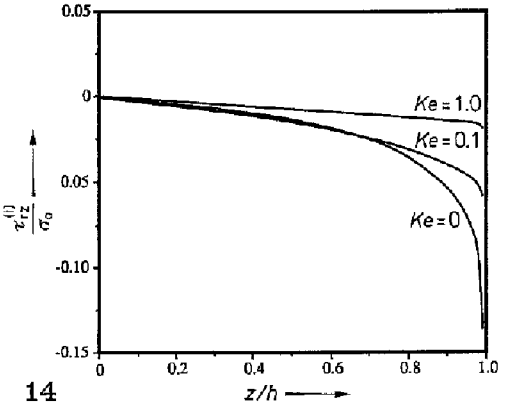

14

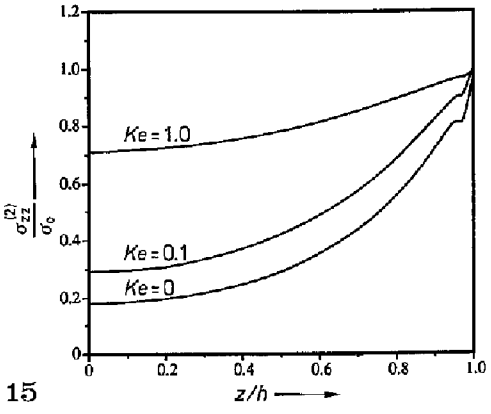

15

Figs. 13–15. **13** Stress σ_{rr} vs z/h, **14** stress τ_{rz} vs z/h, and **15** stress $\sigma_{zz}^{(2)}$ vs z/h, all for imperfect bonding case where $\nu_1 = \nu_2 = 0.33$, $\mu_2/\mu_1 = 17$ and $a/h = 0.05$

a significant change on the stress field can only occur when the coated material is very soft. This suggests, therefore, that the stress field calculated from the physical parameters may be quite closer to that calculated from the perfect bonding model.

Perhaps it is appropriate here to note that the authors are well aware of the shortcomings of this type of condition. However, this part of the investigation was of secondary importance relative to the main objectives of the study. The analysis, however, does provide us with further insight on the phenomenon of fiber/matrix interface friction. Moreover, other friction models too are not immune to shortcomings. For example, Hutchinson and Jenson (1990) recently examined fiber/matrix debonding with two different types of frictions (i) constant friction and (ii) Coulomb friction. Their analysis was based on a 1D cylinder model. However, as one can see from Fig. 6, of the present analysis, the interfacial shear stress, in general, is not constant. If, on the other hand, the matrix is allowed to carry some of the load, which is usually the case, the shear stress does become approximately constant (i.e., zero) as it may be seen in Fig. 11, for $\sigma_i/\sigma_0 = 0.05$. Moreover, as the fiber is allowed to slip more and more, the stress singularity at the edge may ultimately be eliminated in which case the boundary layer region will disappear. Thus, the use of a constant friction law, once slippage has initiated, will be justifiable. But then the spring model also enjoyes the same advantages. The Coulomb friction law also presents some mathematical difficulties. More specifically, the shear stress is an odd function of z while the radial stress is an even function of z. Thus, at $z = 0$, the shear stress vanishes while the radial stress does not! Moreover, at the fiber edge the shear stress vanishes while the radial stress does not. Mathematically, therefore, such a friction law is also peculiar in representing fiber/matrix interface friction prior to slippage. The reader may note, however, that for certain ratios of μ_2/μ_1, the radial stress, as well as the shear stress, are almost zero (see Figs. 10 and 11 for $\sigma_i/\sigma_0 = 0.05$) and the power law in that case is satisfied (Except in the boundary layer region). It is hoped that the above discussion will give the reader a better

understanding of the reasons why we have chosen the use of a spring model in order to obtain some preliminary results on slippage. Be that it may, the subject of friction and sliding is certainly not a trivial one and that further investigation is warranted. Finally, the authors concur with the observation made by Hutchinson and Jenson that the correct characterization of friction sliding of a fiber embedded into a matrix remains an open issue.

5 Comparisons and conclusions

Our present results are consistent with previous observations based on 1D and 2D considerations (Lawrence, 1972 and Banbaji, 1988) that τ_{rz} and $\sigma_{zz}^{(2)}$ will attain their maximum values at the loaded end of the fiber. Although, our present model differs from previous 3D models (Muki et al. 1970; Luk et al. 1979; Haener et al. 1967), the stress profiles obtained are similar. For example, comparing the result of Haener (1965) to that of our perfect bonding model 1, one finds that the stresses $\sigma_{zz}^{(i)}$ and $\sigma_{rr}^{(i)}$ obtained in these two different models both show a flat behavior in the center region (actually the value is rather small in this region for σ_{rr}) and then a sudden jump to a larger value near the edge. In addition, our present numerical results do confirm the presence of a stress singularity in the neighborhood of the fiber edge.

A qualitative explanation of the fiber multiple crack phenomenon found in the Dogbone test samples (DiBenedetto et al. 1986 and Bascom et al. 1986) can be made by examining the fiber tensile stress along its length. Figure 16 shows two curves corresponding to two different geometric ratios $a/h = 0.01$ and $a/h = 0.05$, where $[\sigma]$ denotes the tensile strength of the fiber. As we can see, the tensile strength in a longer fiber ($a/h = 0.01$) has passed the dash line and hence will break

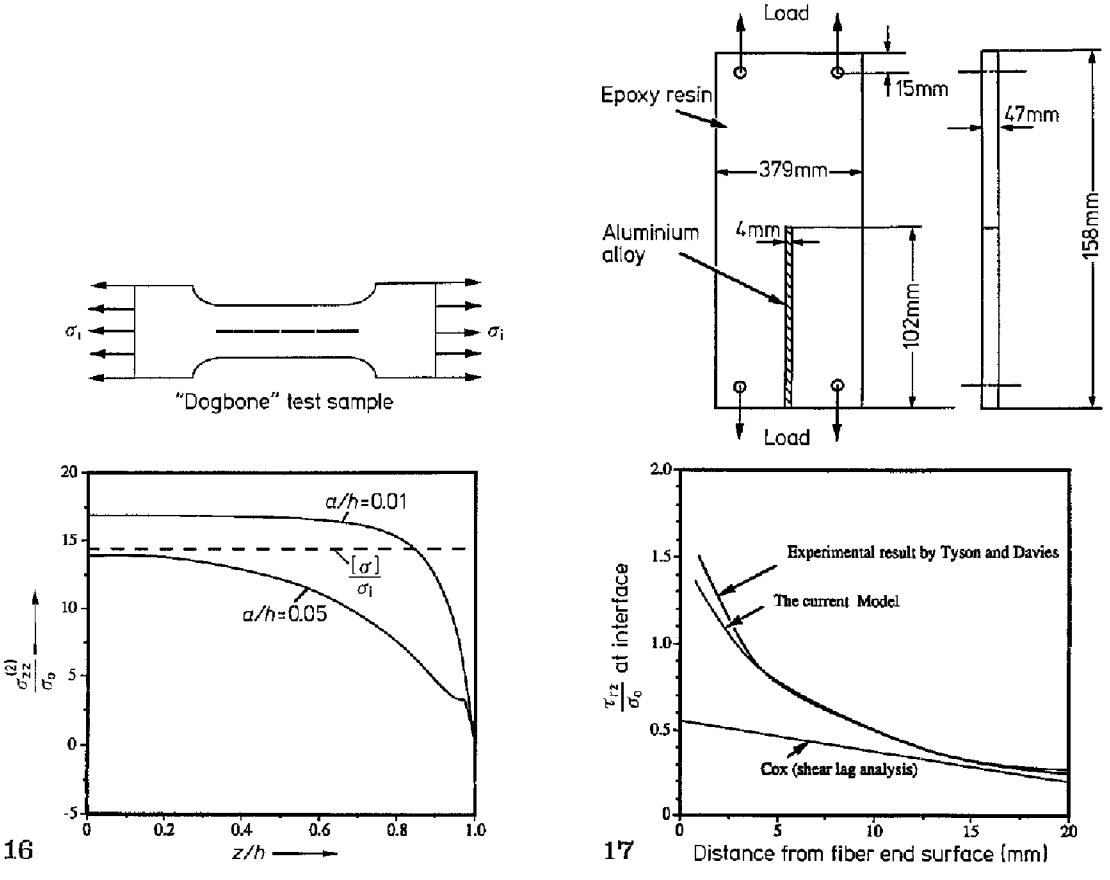

Figs. 16 and 17. **16** Dogbone test sample and the fiber tensile stress vs z/h where $\nu_1 = \nu_2 = 0.33$ and $\mu_2/\mu_1 = 17$. **17** Comparison with the experimental results obtained by Tyson and Davies

while the shorter fiber ($a/h = 0.05$) will not break because the maximum tensile stress is below the dash line. However, if σ_i increases, the dash line will move lower provided that the tensile strength of the fiber is independent of the ratio a/h. This may lead to the breakage of a shorter fiber. It becomes clear that the fiber tends to relax itself by having a shorter length. Another interesting phenomenon is that the non-dimensionalized tensile stress at the fiber center for the case $a/h = 0.01$ is about 17, which is equal to the shear moduli ratio of the current problem. Cox (1952) has predicted that the maximum tensile stress of the fiber under this model will occur at the fiber center and that its value will be $E_2\sigma_i/E_1$. This will yield the value of $17\sigma_i$, if one assumes the Poisson ratio of the fiber and of the matrix to be the same. His prediction, however, becomes inaccurate as the fiber length decreases. This indicates that the $E_2\sigma_i/E_1$ may only be taken as an upper bound of the fiber tensile stress.

A quantitative comparison of the present results with the experimental results obtained by Tyson and Davies (1965) is shown in Fig. 17. The parameters of their 2D experimental model are taken to fit our current 3D model. The diameter of the fiber was taken as 4 mm and the half thickness of the plate h used was the experimentally determined distance from the fiber to the isotropic point (see Tyson and Davies). All other parameters are given in the paper and can be used directly. As seen from the figure, the present results predict the interfacial shear stress very well throughout the interface. A small deviation begins at $x = 4$ mm, i.e., at approximately one fiber diameter away from the fiber end. This deviation was to be expected for the present model does not account for the localized stress riser effect (instead of the uniform applied load) which is present at the vicinity of the fiber end. On the other hand, the experimental results substantiate our previous observation that such a stress riser effect is localized to within a one fiber diameter region. Alternatively, the result predicted by a shear lag analysis greatly underestimates the interfacial shear stress especially in the vicinity of the fiber end.

In view of the above, the following conclusions may now be reached:

(1) The geometric parameter a/h, as well as the material properties, greatly affect the displacement and stress fields and for this reason play a fundamental role on the mechanism of failure.
(2) As expected, a boundary layer effect is shown to prevail in the vicinity of the fiber edge where the presence of a stress singularity (Folias 1989; 1991) may ultimately induce crack initiation.
(3) In general, a shear lag type of analysis may underestimate the magnitude of interfacial shear stress.
(4) When $\sigma_i/\sigma_0 < \mu_1/\mu_2$, interfacial debonding, slippage and fiber breakage most likely will initiate at the edge region.
(5) When $\sigma_i/\sigma_0 > \mu_1/\mu_2$, interfacial slippage will initiate at the edge region while interfacial debonding and fiber breakage will initiate at the center region.
(6) In applications where a stress riser effect is present at the fiber edge (see Fig. 2), the present model predicts accurately the interfacial shear stress except in the vicinity of one fiber diameter away from the fiber edge (see Fig. 17).
(7) If only the fiber is allowed to carry the applied load, then the interfacial shear stress will not be a constant.
(8) If both fiber and matrix are allowed to carry the applied load, then in general the shear stress will not be a constant.
(9) Exception to (8) is the case where the ratio of $\sigma_i/\sigma_0 \cong \mu_2/\mu_1$ in which case both the radial as well as the shear stress are approximately zero except in the vicinity of the fiber edge (see Figs. 10 and 11 for $\sigma_i/\sigma_0 = 0.05$).
(10) The substitution of the "interphase" with an elastic friction law leads to a stress relaxation.
(11) The use of a modified layer (fiber coating) has a minimal effect on the magnitude of the stress field and a great effect on the characterization of the fracture process as adhesive or cohesive (see Zhong's Dissertation 1991).

The analysis also provides some further insight on the subject of interface friction. The reader is referred to the section "Numerical Results".

Next, our research activities are branching out along three different directions. First, we are extending the analysis to the case of a doubly periodic array of fibers. The work is almost completed

and the results will be reported in a follow up paper soon. Second, the fiber has next been allowed to break, at the location $z = 0$, and a fracture analysis based on 3D elasticity considerations is sought. The investigation is well on the way. This problem was recently investigated by Whitney and Drzal (1987) and an approximate closed form solution was developed. Their model provides a substantial improvement over the existing "shear lag" models. However, as the authors point out, in order to evaluate the interface and its role in the composite fracture process, or in determining composite toughness, the 3D stress distribution around the fiber is desired. The work provides important and valuable guidance to our investigation. Third, the 3D consideration of debonding at the fiber/matrix interface is examined. Approximate solutions to this problem may be found in the literature, e.g., Gao et al. (1988), which serve as excellent bases on which to build upon and to complement.

Acknowledgements

This work was supported in part by the Air Force Office of Scientific Research Grant No. AFOSR-90-0351. The author wishes to thank Lt. Col. G. Haritos for this support and for various discussions.

References

Achenbach, J. D.; Zhu, H. (1989): Effect of interfacial zone on mechanical behavior and failure of fiber-reinforced composites. J. of Mech. Phys. Solids, Vol. 37, No. 3, 381–393

Banbaji, J. (1988): On a more generalized theory of the pull-out test from an elastic matrix. Composites Science and Technology 32, 183–193

Bascom, W. D.; Jensen, R. M. (1986): Stress transfer in single fiber/resin tensile tests. J. Adhes. 19, 219–239

Bloom, J. M. (1967): Axial loading of a unidirectional composite. J. Compos. Mater. 1, 268–277

Chua, P. S.; Piggott, M. R. (1985): The glass fiber-polymer interface: II – work of fracture and shear stress. Composites Science and Technology 22, 107–119

Cox, H. L. (1952): The elasticity and strength of papers and other fiberous materials. Br. J. Appl. Phys. 3, 72–79

DiBenedetto, A. T.; Nocolais, L.; Ambrosio, L.; Groeger, J. (1986): Stress transfer and fracture in single fiber/epoxy composites. Proceeding of the first International Conference on Composite Interface 47–54

Dollar, A.; Steif, P. S. (1988): Load transfer in composites with a Coulumb friction interface. Int. J. Solids Struct. 24, 789–803

Folias, E. S. (1975): On the three dimensional theory of cracked plates. J. Appl. Mech. 663–673

Folias, E. S. (1989): On the stress singularities at the intersection of a cylindrical inclusion with the free surface of a plate. Int. J. Fract. 39, 25

Folias, E. S.; Reuter, W. G. (1990): On the equilibrium of a linear elastic layer. Comput. Mech. 5, 459–468

Folias, E. S. (1991): On the prediction of failure at a fiber/matrix interface in a composite subjected to a transverse tensile load. J. Comp. Mater. Vol. 25, 869–886

Gao, Y. C.; Mai, Y. W.; Cotterell, B. (1988): Fracture of fiber-reinforced materials. J. Appl. Math. Phys. Vol. 39, 550–572

Haener, J.; Ashbaugh, N. (1967): Three-dimensional stress distribution in a unidirectional composite. J. Comp. Mater. 1, 54–63

Haritos, G. K.; Keer, L. M. (1985): Pullout of a rigid insert adhesively bonded to an elastic half plane. J. Adhes. 18, 131–150

Hutchinson, J. W.; Jensen, M. H. (1990): Models of fiber debonding and pullout in briltle composites with friction. Mech. Mater. 9, 139–163

Lawrence, P. (1972): Some theoretical considerations of fiber pull-out from an elastic matrix. J. Mater. Science 7, 1–6

Li, C. C.; Folias, E. S. (1991): Edge effect of a carbon fiber meeting a surface. J. Mech. Mater. to appear

Luk, V. K.; Keer, L. M. (1979): Stress analysis for an elastic half space containing an axially-loaded rigid cylindrical rod. Int. J. Solids Struct. 15, 805–827

Muki, R.; Sternberg, E. (1970): Elastostatic load-transfer to a half-space from a partially embedded axially loaded rod. Int. J. Solids Struct. 6, 69–90

Penado, F. E.; Folias, E. S. (1989): The three dimensional stress field around a cylindrical inclusion in a plate of arbitrary thickness. Int. J. Fract. 39, 129–145

Penn, L. S.; Lee, S. M. (1989): Interpretation of experimental results in the single pull-out filament test. J. Composites Technology and Research 11, 23–30

Sendeckyj, G. P. (1970): Elastic inclusion problems in plane elastostatic. Int. J. Solids Struct. 6, 1535–1543

Steif, P. S.; Hoysan, S. F. (1986): On load transfer between imperfectly bonded interface. Mech. Mater. 5, 375–382

Tyson, Davies, G. J. (1965): A photoelastic study of the shear stress associated with the transfer of stress during fiber reinforcement. Br. J. Appl. Phys. 16, 199–205

Williams, M. L. (1952): Stress singularities resulting from various boundary conditions in angular corners of plates in extension. J. Appl. Mech. 74, 526

Whitney, J. M.; Drzal, L. T. (1987): Axisymmetric stress distribution around an isolated fiber fragment. ASTM STP 937, 179–196

Yu, I. W.; Sendeckyj, G. P. (1974): Multiple circular inclusion problems in plane elastostatic. J. Appl. Mech. 41, 215–221

Zhong, F. H. (1991): PhD dissertation, U. of Utah, Department of Mechanical Engineering

Communicated by S. N. Atluri, October 21, 1991